

Exploring the QCD landscape with high-energy nuclear collisions

Bedangadas Mohanty

Variable Energy Cyclotron Centre, 1/AF, Bidhan Nagar, Kolkata - 700064, India

E-mail: bmohanty@vecc.gov.in

Abstract. Quantum chromodynamics (QCD) phase diagram is usually plotted as temperature (T) versus the chemical potential associated with the conserved baryon number (μ_B). Two fundamental properties of QCD, related to confinement and chiral symmetry, allows for two corresponding phase transitions when T and μ_B are varied. Theoretically the phase diagram is explored through non-perturbative QCD calculations on lattice. The energy scale for the phase diagram ($\Lambda_{\text{QCD}} \sim 200$ MeV) is such that it can be explored experimentally by colliding nuclei at varying beam energies in the laboratory. In this paper we review some aspects of the QCD phase structure as explored through the experimental studies using high energy nuclear collisions. Specifically, we discuss three observations related to the formation of a strongly coupled plasma of quarks and gluons in the collisions, experimental search for the QCD critical point on the phase diagram and freeze-out properties of the hadronic phase.

PACS numbers: 25.75.-q, 25.75.Nq, 12.38.Mh, 25.75.Ag, 25.75.Bh, 25.75.Dw, 25.75.Gz, 25.75.Ld

Keywords: Quark Gluon Plasma, Strangeness enhancement, Jet quenching, Elliptic flow, Chemical and kinetic freeze-out, QCD phase diagram and QCD critical point.

1. QCD Phase Diagram

Physical systems undergo phase transitions when external parameters such as the temperature (T) or a chemical potential (μ) are changed. A phase diagram provides intrinsic knowledge on the structure of the matter under study. In other words, it tells us how matter organizes itself under external conditions at a given degrees of freedom. The theory of strong interactions, QCD, predicts that nuclear matter at high temperature and/or density makes a transition from a state where quarks and gluons are confined and chiral symmetry is broken to a state where quarks and gluons are de-confined and chiral symmetry is restored [1]. QCD has several conserved quantities: baryon number (B), electric charge (Q), and strangeness (S). Each of these is associated with a chemical potential. As a result, the QCD phase diagram is four-dimensional. μ_Q and μ_S are relatively small compared to μ_B (baryonic chemical potential) in high energy nuclear collisions [2]. The T and μ_B are varied in a typical QCD phase diagram

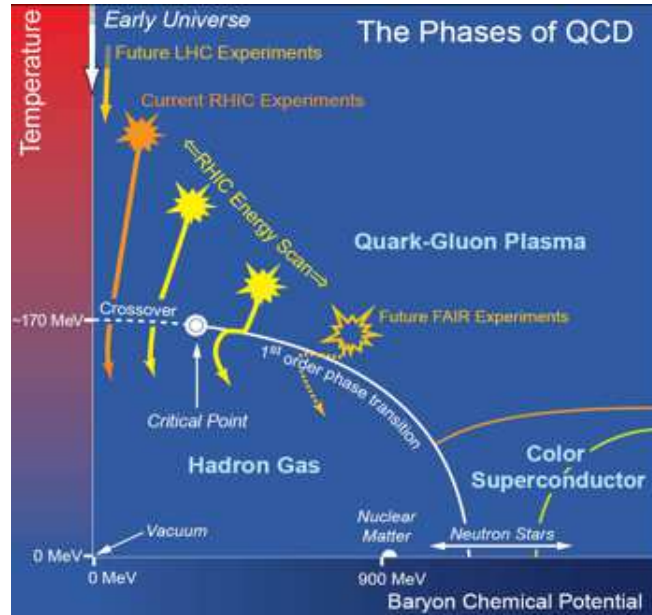


Figure 1. (Color online) Typical phase diagram of QCD. See text for details. Figure taken from Ref. [3].

as shown in Fig. 1 [3]. At high temperature and density the phase is governed by quark and gluon degrees of freedom and is commonly referred to as the Quark Gluon Plasma (QGP) [4]. At large densities and low temperatures other interesting phases related to neutron star [5] and color superconductivity [6] starts to appear. These QCD transitions which occurred in the early universe have the right energy scale to be accessible by the experiments. The Fig. 1 shows the parts of the phase diagram explored by several accelerator based experimental programs. Experimentally, this is done by varying the beam energy. Both, T and μ_B , vary as the function of the center-of-mass energy ($\sqrt{s_{NN}}$) [7]. This strategy is being followed by experimental programs at Large Hadron Collider (LHC) at CERN, Relativistic Heavy Ion Collider (RHIC) at BNL and Super Proton Synchrotron (SPS) at CERN, and will be followed at Facility for Antiproton and Ion Research (FAIR) at GSI and Nuclotron-based Ion Collider fAcility (NICA) at JINR. Among these experiments, we discuss in section 2, selected results from RHIC which provides evidence for the formation of a QGP [8].

Theoretically, finite temperature lattice QCD calculations at $\mu_B = 0$ suggest a cross-over [9] above a temperature, T_c , of about 170 to 190 MeV from a system with hadronic degrees of freedom to a QGP [10]. At large μ_B , several QCD based calculations find the quark-hadron phase transition to be of first order [11]. Going towards the smaller μ_B region, the point in the QCD phase plane (T vs. μ_B) where the first order phase transition ends is the QCD Critical Point (CP) [12]. The focus in the coming decade would be on attempts to locate the CP both experimentally and theoretically. Current theoretical calculations are highly uncertain about the location of the CP. This is primarily because the lattice QCD calculations at finite μ_B face numerical challenges.

The experimental plan (discussed in section 3) is to vary the $\sqrt{s_{\text{NN}}}$ of heavy-ion collisions to scan the phase plane and, at each energy, search for signatures of the CP that might survive the evolution of the system. In the last section of the review we discuss the thermodynamic properties of the hadronic phase. Finally we end with a summary of our current understanding of phase diagram and a brief outlook.

2. Establishing the Partonic Phase at RHIC

2.1. Strangeness enhancement and formation of a gluon rich plasma

Enhancement of strange hadron production in high energy heavy-ion collisions [13] due to formation of QGP is one of the four classic signatures in this field. The other three being, enhanced direct photon [14] and dilepton [15] production and suppression of J/Ψ production [16] in heavy-ion collisions relative to $p+p$ collisions. In a QGP, thermal s and \bar{s} quarks can be produced by gluon-gluon interactions [17]. These interactions could occur very rapidly and the s -quark abundance would equilibrate. During hadronisation, the s and \bar{s} quarks from the plasma coalesce to form ϕ mesons. Production by this process is not suppressed as per the OZI (Okubo-Zweig-Izuka) rule [18]. This, coupled with large abundances of strange quarks in the plasma, may lead to a dramatic increase in the production of ϕ mesons and other strange hadrons relative to non-QGP $p+p$ collisions.

Such predictions of relative enhancement of strange hadron was challenged by an alternate idea of canonical suppression of strangeness in small systems being the source of strangeness enhancement in Λ , Ξ and Ω hadrons in high energy heavy-ion collisions [19]. The strangeness conservation laws require the production of an \bar{s} -quark for each s -quark in the strong interactions. The main argument in such canonical models is that the energy and space time extensions in smaller systems may not be sufficiently large. This leads to a suppression of open-strange hadron production in small collision systems. These statistical models fit the data reasonably well [20]. These models predict two things: (a) strangeness enhancement in nucleus-nucleus collisions, relative to $p+p$ collisions, should increase with the valence strange quark content of the hadrons and (b) the enhancement is predicted to decrease with increasing beam energy [21]. Discriminating between the two scenarios, QGP versus the canonical suppression, using the experimental data on K^\pm , Λ , Ξ and Ω hadrons has been, to some extent, ambiguous. Enhancement of $\phi(s\bar{s})$ production (zero net-strangeness, hence not subjected to the canonical suppression) in heavy-ion collisions relative to $p+p$ collisions would clearly indicate the formation of a gluon rich QGP in these collisions. This would then rule out canonical suppression scenario.

Figure 2 shows the enhancement of strange hadron production at RHIC [22]. Upper panel shows the ratio of strange hadron production normalized to $\langle N_{\text{part}} \rangle$ in nucleus-nucleus collisions relative to corresponding results from $p+p$ collisions at 200 GeV. The results are plotted as a function of $\langle N_{\text{part}} \rangle$. K^- , $\bar{\Lambda}$ and $\Xi + \bar{\Xi}$ are found to exhibit an

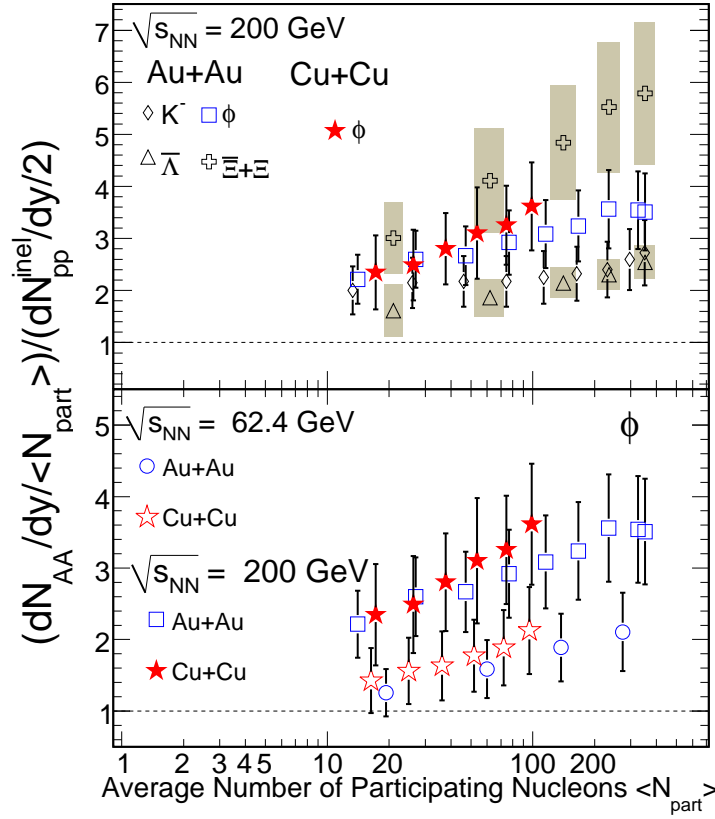


Figure 2. (Color online) Upper panel: The ratio of the yields of K^- , ϕ , $\bar{\Lambda}$ and $\Xi + \bar{\Xi}$ normalized to average number of participating nucleons ($\langle N_{part} \rangle$) in nucleus-nucleus collisions to corresponding yields in inelastic $p+p$ collisions as a function of $\langle N_{part} \rangle$ at 200 GeV. Lower panel: Same as above for ϕ mesons in Cu+Cu collisions at 200 and 62.4 GeV. The $p+p$ collision data at 200 GeV are from STAR experiment and at 62.4 GeV from ISR [23]. The error bars shown represent the statistical and systematic errors added in quadrature. Figure is taken from Ref. [22].

enhancement (value > 1) that increases with the number of strange valence quarks. Furthermore, the observed enhancement in these open-strange hadrons increases with collision centrality, reaching a maximum for the most central collisions. However, the enhancement of ϕ meson production shows a deviation from the ordering in terms of the number of strange constituent quarks. More explicitly, this enhancement is larger than for K^- and $\bar{\Lambda}$, at the same time being smaller than in case of $\Xi + \bar{\Xi}$. Despite being different particle types (meson-baryon) and having different masses, the results for K^- and $\bar{\Lambda}$ are very similar in the entire centrality region studied. This rules out a baryon-meson effect as being the reason for the deviation of ϕ mesons from the number of strange quark ordering seen in Fig. 2 (upper panel). The observed deviation is also not a mass effect as the enhancement in ϕ meson production is larger than that in $\bar{\Lambda}$ (which has mass close to that of the ϕ). Further in heavy-ion collisions, the production of ϕ mesons is not canonically suppressed due to its $s\bar{s}$ structure.

The observed enhancement of ϕ meson production then is a clear indication for the formation of a dense partonic medium being responsible for the strangeness enhancement in Au+Au collisions at 200 GeV. The observed enhancement in ϕ meson production being related to medium density is further supported by the energy dependence shown in the lower panel of Fig. 2. The ϕ meson production relative to $p+p$ collisions is larger at higher beam energy, a trend opposite to that predicted in canonical models for other strange hadrons. In addition measurements have shown that ϕ meson production is not from the coalescence of $K\bar{K}$ and is minimally affected by re-scattering effects in the medium [24]. Measurements also indicate that ϕ mesons are formed from the coalescence of seemingly thermalized strange quarks [25]. All these observations put together indicate the formation of a dense partonic medium in heavy-ion collisions where strange quark production is enhanced. This in turn suggests that the observed centrality dependence of the enhancement for other strange hadrons (seen in Fig. 2) is likely to be related to the same reasons as in the case of the ϕ meson, that it is due to the formation of a dense gluon rich partonic medium in the collisions. These experimental data rule out the possibility of canonical suppression being the only source of the observed strangeness enhancement at $\sqrt{s_{NN}} = 200$ GeV.

2.2. Jet Quenching and highly opaque medium

One of the most exciting results to date at RHIC is the discovery of suppression in the production of high transverse momentum (p_T) mesons in nucleus-nucleus collisions compared to corresponding data from the binary collision scaled $p+p$ collisions [26]. This has been interpreted in terms of energy loss of partons in QGP. This phenomena is called as the jet quenching in a dense partonic matter [27]. The energy loss by energetic partons traversing the dense medium formed in high-energy heavy-ion collisions is predicted to be proportional to both the initial gluon density [28] and the lifetime of the dense matter [29]. The results on high- p_T suppression are usually presented in terms of the nuclear modification factor (R_{AA}), defined as:

$$R_{AA} = \frac{dN_{AA}/d\eta d^2p_T}{T_{AB}d\sigma_{NN}/d\eta d^2p_T} \quad (1)$$

where the overlap integral $T_{AB} = N_{binary}/\sigma_{inelastic}^{pp}$ with N_{binary} being the number of binary collisions commonly estimated from Glauber model calculation [30].

In Fig. 3 we show the RHIC data for the $R_{AA}(p_T)$, for various produced mesons [31] and direct photons [32] in central Au+Au collisions at midrapidity. A large suppression in high p_T meson production is observed, and those for π^0 's being almost flat at $R_{AA} \simeq 0.2$ up to 20 GeV/c. The figure also shows that the level of suppression for π^0 's, η 's and ϕ -mesons are very similar, which supports the conclusion that the suppression occurs in the partonic phase, not in the hadronic phase. This strong suppression of meson production is in contrast to the behavior of direct photons, also shown in the figure. The direct photons follow binary scaling (i.e. $R_{AA} \simeq 1$) or no suppression. This is a strong evidence that the suppression is not an initial state effect, but a final state

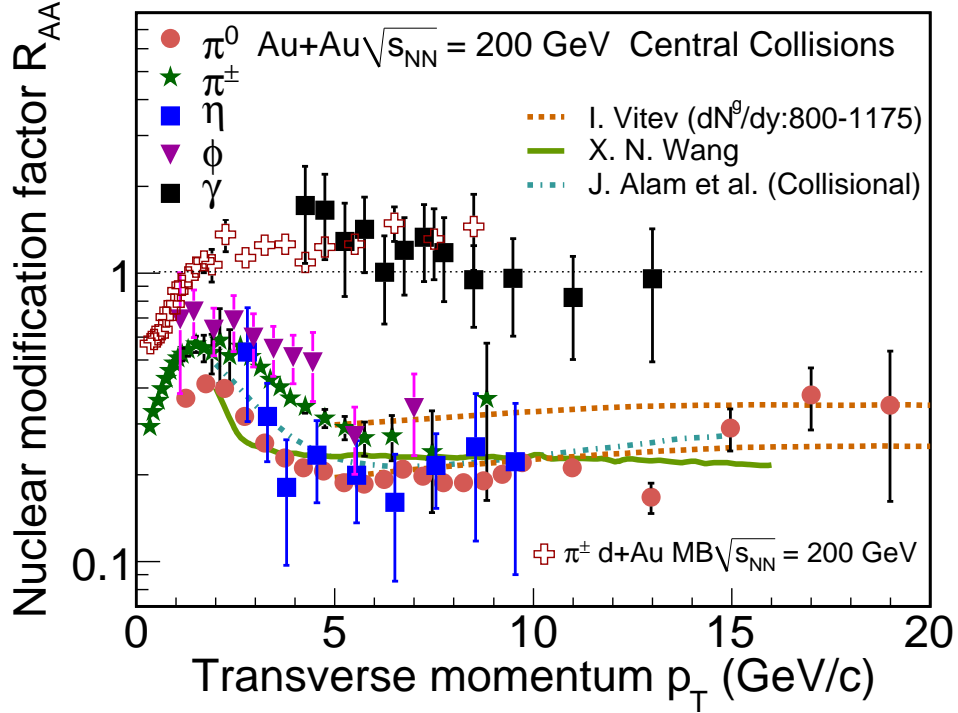


Figure 3. (Color online) Compilation of the nuclear modification factor (R_{AA}) for mesons and direct photons as measured in RHIC experiments at midrapidity for central Au+Au collisions at $\sqrt{s_{NN}} = 200$ GeV. Also shown are the R_{dAu} for charged pions for $\sqrt{s_{NN}} = 200$ GeV. The lines are results from various model calculations. See text for more details.

effect caused by the high density medium with color charges created in the collision. This is further consolidated by a demonstration through a controlled experiment using deuteron on Au ion collisions, which gave a $R_{dAu}(p_T) \sim 1$ for π^\pm at midrapidity and high p_T [33].

The various curves in the Fig. 3 represents different model calculations. The dashed curve shows a theoretical prediction using the GLV parton energy loss model [28]. The model assumes an initial parton density $dN/dy = 800 - 1100$, which corresponds to an energy density of approximately 5-15 GeV/fm³. The lower dashed curves are for higher gluon density. The precision high p_T data at RHIC has been used to characterize medium density fairly accurately. The conclusion being that the medium formed in central Au+Au collisions at RHIC has a high degree of opacity [34]. In addition, theoretical studies suggest that for a given initial density, the $R_{AA}(p_T)$ values are also sensitive to the lifetime (τ) of dense matter formed in heavy-ion collisions [29]. The solid curves are predictions from Ref. [29] at $\sqrt{s_{NN}} = 200$ GeV with $\tau = 10$ fm/c (i.e. larger than the typical system size of $\sim 6-7$ fm). The parton energy loss calculations discussed above attributes the opacity to plasma induced radiation of gluons, much like

ordinary bremsstrahlung of photons by electrons. However, the quantitatively large suppression pattern observed at high p_T , for both light hadrons and those involving heavy quarks [35], showed that the mechanism of energy loss is far from being a settled issue, namely, the relative contribution of radiative and collisional forms. As an example, shown in Fig. 3 is a comparison of the data to theoretical results (dot-dash curves) on R_{AA} from models that consider only collisional energy loss [36]. This model gives R_{AA} values at high p_T close to the measured values and similar to corresponding values from models having only a radiative mechanism for parton energy loss.

Leading particle measurements, such as the ones shown in Fig. 3 suffer from a number of limitations. (a) Leading hadrons come from a mixture of parent quarks and gluons. (b) As a fragmentation product, the energy of a leading hadron is not a perfect proxy for the energy of the parent parton as it samples a wide range of partonic energies. In future we should look forward to potentially three interesting measurements. (i) The γ -jet process potentially provides access to the underlying scattered parton's energy. Measurements of the distribution of particles from the jet opposite, in azimuth, to the tagged photon reveals how much energy was lost, and how it was redistributed, by the colored parton as it traversed the medium [37]. (ii) Another method is through the full reconstruction of jets in heavy-ion collisions [38]. Beyond producing a far better proxy for the energy of the parent parton than a leading hadron, this technique allows one to trace the evolution of energy flow in directions both longitudinal and transverse to the direction of the parent parton. Both these methods are under active pursuit at RHIC. (iii) Another important feature of jet quenching is provided by partonic identity. While it is difficult to disentangle light quarks from gluons, especially in a heavy-ion environment, charm and bottom can be easily tagged by the existence of a charmed or bottom hadron in the final state. Due to their large masses the charm and bottom quarks are predominantly produced via hard scattering in the initial stage of the high-energy heavy-ion collision. The final state spectra can therefore serve as a sensitive tool to probe in-medium rescattering and interactions responsible for thermalization. This will also allow to study the non-Abelian feature of QCD that results in the gluons losing more energy than quarks in the medium [39]. Plans are in place to measure the cross-sections and transverse momentum spectra of hadrons with open and hidden heavy flavor at RHIC with new detector upgrades. This will also provide useful data to understand the different mechanisms of energy loss: collisional versus radiative.

2.3. Partonic collectivity and low viscosity

Elliptic flow, v_2 , is an observable which is thought to reflect the conditions from the early stage of the collisions [40]. In non-central heavy-ion collisions, the initial spatial anisotropy of the overlap region of the colliding nuclei is transformed into an anisotropy in momentum space through interactions between the particles. As the system expands it becomes more spherical, thus the driving force quenches itself. Therefore the elliptic flow is sensitive to the collision dynamics in the early stages. It is measured, by

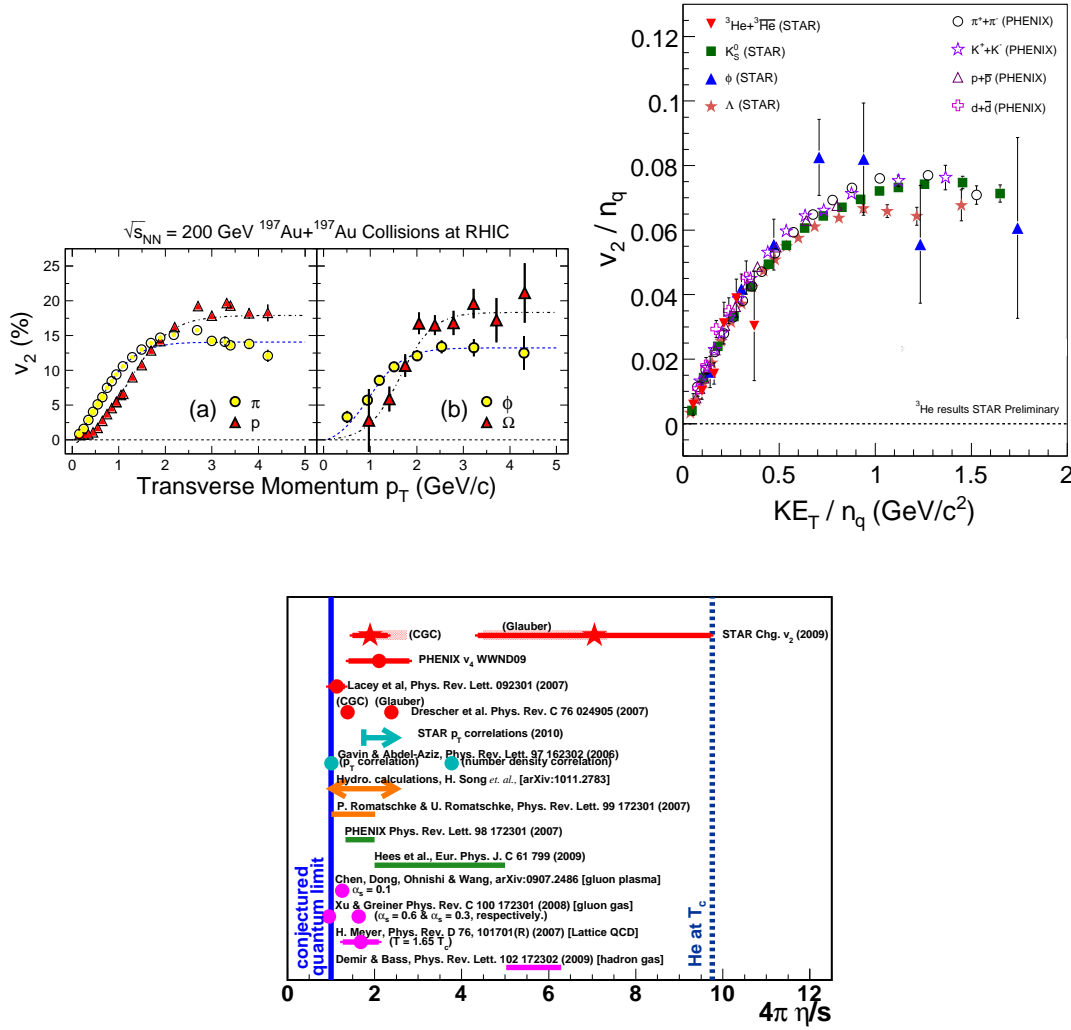


Figure 4. (Color online) Top left plot: The elliptic flow v_2 for (a) light quark hadrons and (b) strange quark hadrons. The data is from the minimum bias Au+Au collisions at midrapidity for $\sqrt{s_{NN}} = 200$ GeV [41]. Top right plot: Compilation of the number of constituent quark scaled v_2 as a function of the scaled transverse kinetic energy [42]. Bottom plot: Compilation of η/s extracted from various measurements in heavy-ion collisions at RHIC.

calculating $\langle \cos(2(\phi - \Psi)) \rangle$, where ϕ is the azimuthal angle of the produced particles and Ψ is the azimuthal angle of the impact parameter, and angular brackets denote an average over many particles and events.

Figure 4 top left panel shows the RHIC results on v_2 of light quark (π and p) and strange quark (ϕ and Ω) carrying hadrons in Au+Au collisions at 200 GeV [41]. Three very distinct experimental observations can be made. (a) At low p_T (< 2 GeV/c) the heavier hadrons have smaller v_2 . Such a mass ordering is expected in hydrodynamics calculations of $v_2(p_T)$ for identified particles [43]. (b) At the intermediate p_T range of 2-5 GeV/c it is observed that baryons have higher v_2 than mesons. The ϕ -meson v_2 plays a

crucial role in establishing this baryon-meson difference. Such a separation of baryons and mesons in the intermediate p_T range has been also observed in measurements of the nuclear modification factor, R_{CP} [44]. These results are consistent with calculations from quark recombination models [45] implying the de-confinement of the system prior to hadronisation. (c) Comparison between the v_2 results for light quark carrying hadrons to those from strange quark carrying hadrons indicates both types of hadrons show similar magnitude of v_2 . The multi-strange hadrons (ϕ and Ω) have relatively low hadronic interaction cross sections and freeze-out early, hence are considered as the most promising probes of the early stages of the collision. All the above results indicates that a substantial amount of collectivity has been developed at the partonic stage of the heavy-ion collisions. In fact none of the available hadronic models are able to account for the observed magnitude of v_2 at $\sqrt{s_{NN}} = 200$ GeV. Only models which have additional partonic interactions explain the $\langle v_2 \rangle$ values [46].

When elliptic flow v_2 is plotted versus transverse kinetic energy $(m_T - m_0)$, both divided by the number of constituent quarks, the v_2 for all identified hadrons as well as light nuclei below $(m_T - m_0) \sim 1$ GeV/ c^2 falls on a universal curve [47]. m_0 is the mass of the particle. This scaling behavior as shown in Fig.4 further strengthens the evidence for formation of partonic matter during the Au + Au collision process at 200 GeV. It is very hard to explain this observed pattern in a scenario where only hadronic matter exists throughout the interaction, whereas the hypothesis of coalescence of hadrons from de-confined quarks offers a ready explanation. Turn-off of the scaling at a given beam energy would indicate the hadronic side of the phase boundary.

The v_2 measurements of light quark carrying hadrons, the nuclear modification factor and v_2 for heavy quark carrying hadrons and the differential p_T correlations for charged hadrons have been used to extract information of a dimensionless ratio, shear viscosity to entropy (η/s), for the medium formed in heavy-ion collisions at RHIC [48]. Figure 4 bottom panel shows the compilation of η/s extracted from various measurements [49]. It is observed to lie between that conjectured from quantum theory ($\eta/s \sim 1/4\pi$) and those for liquid Helium at T_c . Such a low value of η/s (within a factor 1-10 of the quantum limit) indicates that the matter formed in heavy-ion collisions at RHIC has low viscosity, hence is a strongly coupled system.

3. QCD critical point and thermalization

The CP is a landmark point in the QCD phase diagram, observation of which will make the QCD phase diagram a reality. A close collaboration between the experiments and theory perhaps will lead to its discovery. The first step in this process is to establish an observable for CP which can be measured experimentally and can be related to QCD calculations. In this context, it is important to recall that for a static, infinite medium, the correlation length (ξ) diverges at the CP. ξ is related to various moments of the distributions of conserved quantities such as net-baryons, net-charge, and net-strangeness [50]. Typically variances ($\sigma^2 \equiv \langle (\Delta N)^2 \rangle$; $\Delta N = N - M$; M is the mean) of

these distributions are related to ξ as $\sigma^2 \sim \xi^2$ [51]. Finite size and time effects in heavy-ion collisions put constraints on the values of ξ . A theoretical calculation suggests $\xi \approx 2\text{-}3\text{ fm}$ for heavy-ion collisions [52]. It was recently shown that higher moments of distributions of conserved quantities, measuring deviations from a Gaussian, have a sensitivity to CP fluctuations that is better than that of σ^2 , due to a stronger dependence on ξ [53]. The numerators in skewness ($S = \langle(\Delta N)^3\rangle/\sigma^3$) goes as $\xi^{4.5}$ and kurtosis ($\kappa = [\langle(\Delta N)^4\rangle/\sigma^4] - 3$) goes as ξ^7 . A crossing of the phase boundary can manifest itself by a change of sign of S as a function of energy density [53, 54].

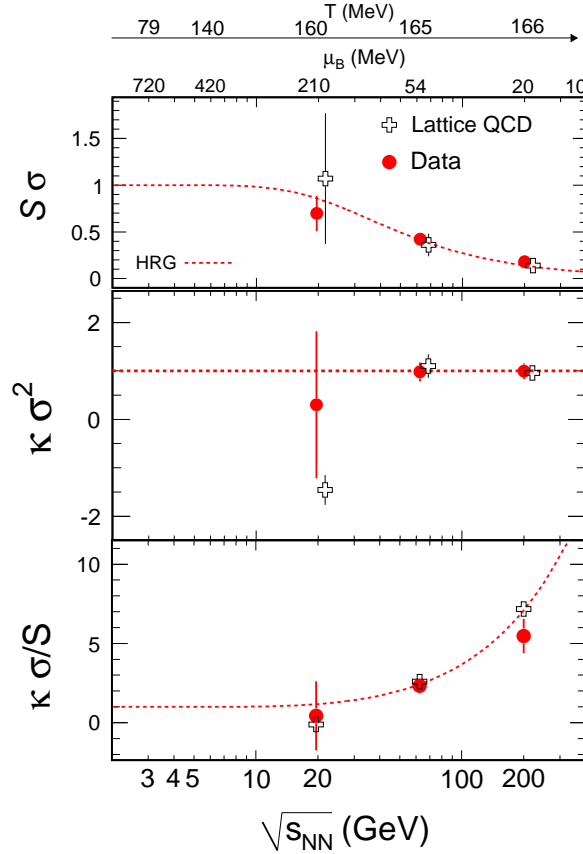


Figure 5. (Color online) $\sqrt{s_{NN}}$ dependence of $S\sigma$, $\kappa\sigma^2$ and $\frac{\kappa\sigma}{S}$ for net-proton distributions measured at RHIC [55]. The results are compared Lattice QCD calculations [56] and HRG model [57]. Also shown on the top are the temperature and baryon chemical potential values at chemical freeze-out extracted from particle yields using a thermal model.

The first connections between QCD calculations and experiment has been recently made [55]. Lattice calculations and QCD-based models show that moments of net-baryon distributions are related to baryon number (ΔN_B) susceptibilities ($\chi_B = \frac{\langle(\Delta N_B)^2\rangle}{VT}$; V is the volume) [56, 58]. Then one can construct ratios such as:

$$S\sigma = \frac{T\chi_B^{(3)}}{\chi_B^{(2)}}, \kappa\sigma^2 = \frac{T^2\chi_B^{(4)}}{\chi_B^{(2)}} \quad \text{and} \quad \frac{\kappa\sigma}{S} = \frac{T\chi_B^{(4)}}{\chi_B^{(3)}},$$

which do not contain the volume and therefore provide a direct and convenient comparison of experiment and theory. In the above expressions the left hand side of each equality can be measured in an experiment whereas the right hand side can be calculated by lattice QCD. Close to the CP models predict the ΔN_B distributions to be non-Gaussian and susceptibilities to diverge causing the experimental observables to have large values. The experimental values should also be compared to those expected from statistics, for example if the p and \bar{p} distributions are individually Poissonian then $\kappa\sigma^2$ for net-protons is unity.

Experimentally measuring event-by-event net-baryon number is difficult. However, the net-proton multiplicity ($N_p - N_{\bar{p}} = \Delta N_p$) distribution is measurable. Theoretical calculations have shown that ΔN_p fluctuations reflect the singularity of the charge and baryon number susceptibility as expected at the CP [59]. Non-CP model calculations show that the inclusion of other baryons does not add to the sensitivity of the observable [55].

Figure 5 shows the energy dependence of $S\sigma$, $\kappa\sigma^2$ and $\frac{\kappa\sigma}{S}$ for ΔN_p , compared to lattice QCD [56] and Hadron Resonance Gas (HRG) model which does not include a CP [57]. The experimental values plotted are for central Au+Au collisions for $\sqrt{s_{NN}} = 19.6, 62.4$ and 200 GeV. The lattice calculations, which predict a CP around $\mu_B \sim 300$ MeV, are carried out using two-flavor QCD with number of lattice sites in imaginary time to be 6 and mass of pion around 230 MeV [56]. The ratios of the non-linear susceptibilities at finite μ_B are obtained using Padé approximant resummations of the quark number susceptibility series. The freeze-out parameters as a function of $\sqrt{s_{NN}}$ are from [60] and $T_c = 175$ MeV.

From comparisons of the experimental data to the HRG model and the lack of non-monotonic dependence of $\kappa\sigma^2$ on $\sqrt{s_{NN}}$ studied, one concludes that there is no indication from the current measurements at RHIC for a CP in the region of the phase plane with $\mu_B < 200$ MeV. Although it must be noted that the errors on the experimental data point at 19.6 GeV is quite large due to small event statistics. It is difficult to rule out the existence of CP for the entire μ_B region below 200 MeV. The extent to which these results can do that is guided by the theoretical work. In addition, the expectation of the extent of the critical region in μ_B is thought to be about 100 MeV. The results discussed here form the baseline for the future CP search program at RHIC [61]. However the fact that the data shows excellent agreement with HRG and Lattice QCD, both of which assume thermalization, is another non-trivial indication of attainment of thermalization (some other measurements are discussed in next section) in heavy-ion collisions. Such a conclusion is drawn for the first time using fluctuation measurements.

With the idea that the rise and then fall of observables sensitive to CP as μ_B increases should allow us to ascertain the (T, μ_B) coordinates of the critical point, the beam energy scan program at RHIC has started. The first phase of the experimental program at RHIC is expected to be completed in 2010-2011. This phase is expected to cover a $\sqrt{s_{NN}}$ region of 39 to 5.5 GeV, which corresponds to a μ_B range of 112 to 550 MeV [62].

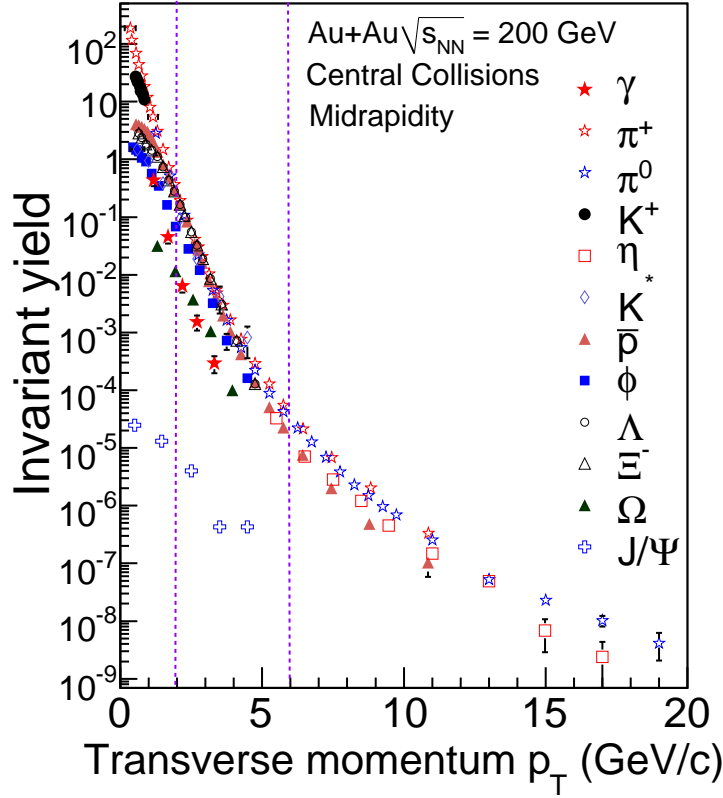


Figure 6. (Color online) Compilation of invariant yield of produced particles at midrapidity versus p_T in central Au+Au collisions at $\sqrt{s_{NN}} = 200$ GeV [2, 25, 31, 32, 63]. The lines show the possibility of having three regions in the spectra where the dominant mechanism of particle productions are different. See text for more details.

4. Hadronic Phase

The measured hadron spectra reflect the properties of the bulk matter at kinetic freeze-out, after elastic collisions among the hadrons have ceased. More direct information on the earlier stages can be deduced from the integrated yields of the different hadron species, which change only via inelastic collisions. The point in time at which these inelastic collisions cease is referred to as chemical freeze-out, which takes place before kinetic freeze-out. RHIC experiments have measured the p_T distribution of variety of particles over a wide range of p_T at midrapidity. A sample of the invariant yield ($\frac{d^2N}{(2\pi p_T)dydp_T}$ (GeV/c) $^{-2}$) of produced particles at RHIC for central Au+Au collisions at $\sqrt{s_{NN}} = 200$ GeV [2, 25, 31, 32, 63] is shown in Fig. 6. Like the p_T dependence of v_2 discussed in the section 2.3, here also we can separate the spectra into 3 regions based on the dominant mechanism of particle production. The low p_T (< 2 GeV/ c) is explained by thermal model based calculations [64], intermediate p_T (2-6 GeV/ c)

by parton recombination based approaches [45] and high p_T (> 6 GeV/ c) by including pQCD based processes or jet production [28, 29]. The only statistical distribution which so far seems to successfully describe the p_T spectra and $v_2(p_T)$ over a wide momentum range is the one based on Tsallis statistics [65].

In this section we concentrate on low p_T part of the spectra for rest of the discussions. The transverse momentum distributions of the different particles contain two components, one random and one collective. The random component can be identified as the one that depends on the temperature of the system at kinetic freeze-out (T_{fo}). The collective component, which arises from the matter density gradient from the center to the boundary of the fireball created in high-energy nuclear collisions, is generated by collective flow in the transverse direction, and is characterized by its velocity β_T . Assuming that the system attains thermal equilibrium, the blast-wave (BW) formulation [66] can be used to extract T_{fo} and $\langle\beta_T\rangle$. The transverse flow velocity of a particle at a distance r from the center of the emission source, as a function of the surface velocity (β_s) of the expanding cylinder, is parameterized as $\beta_T(r) = \beta_s(r/R)^n$, where n is found by fitting the data. The transverse momentum spectrum is then

$$\frac{dN}{p_T dp_T} \propto \int_0^R r dr m_T I_0 \left(\frac{p_T \sinh \rho(r)}{T_{fo}} \right) \times K_1 \left(\frac{m_T \cosh \rho(r)}{T_{fo}} \right),$$

where I_0 and K_1 are modified Bessel functions and $\rho(r) = \tanh^{-1} \beta_T(r)$.

Fits to the identified hadrons p_T distributions at midrapidity for Au+Au collisions at $\sqrt{s_{NN}} = 200$ GeV using Eq. 2 are carried out. The extracted model parameters characterizing the random (generally interpreted as a kinetic freeze-out temperature T_{fo}) and collective (radial flow velocity $\langle\beta_T\rangle$) are shown in Fig. 7 in terms of confidence level (χ^2) contours, for various impact parameters of the collision. As the collisions become more and more central, the bulk of the system, dominated by the yields of π, K, p have lower kinetic freeze-out temperature and develops stronger collective flow. On the other hand, even for the most central collisions, the spectra for multi-strange particles ϕ and Ω appear to reflect a higher freeze-out temperature.

Within a statistical model in thermodynamical equilibrium, the particle abundance in a system of volume V can be given by

$$N_i/V = \frac{g_i}{(2\pi)^3} \gamma_S^{S_i} \int \frac{1}{\exp \left(\frac{E_i - \mu_B B_i - \mu_S S_i}{T_{ch}} \right) \pm 1} d^3p, \quad (2)$$

where N_i is the abundance of particle species i , g_i is the spin degeneracy, B_i and S_i are the baryon number and strangeness number, respectively, E_i is the particle energy, and the integral is taken over all momentum space [2]. The model parameters are the chemical freeze-out temperature (T_{ch}), the baryon (μ_B) and strangeness (μ_S) chemical potentials, and the *ad hoc* strangeness suppression factor (γ_S). Measured particle ratios are used to constrain the values of T_{ch} and μ_B at chemical freeze-out.

Figure 7 compares STAR measurements of integrated hadron yield ratios for central Au+Au collisions to statistical model calculations. The excellent agreement between data and model are observed. The ratios which include stable and long-lived

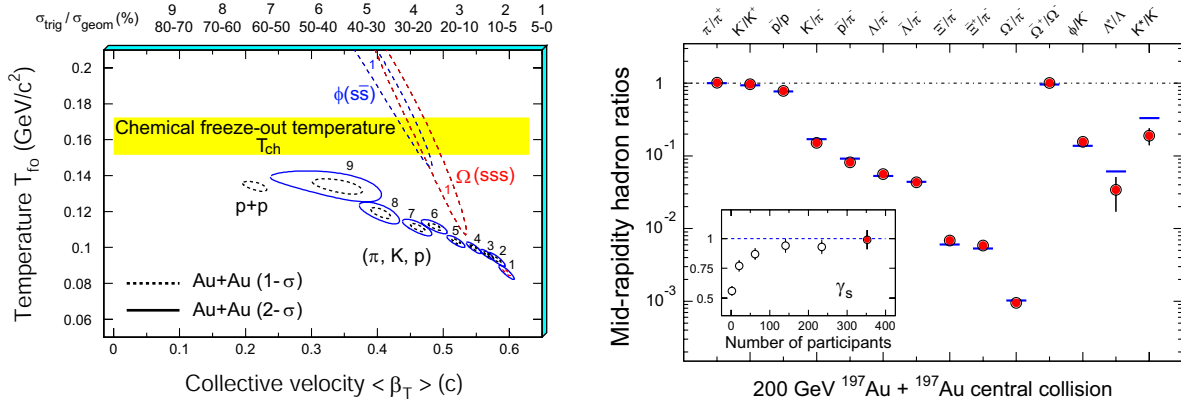


Figure 7. (Color online) Left plot: The χ^2 contours, extracted from thermal + radial flow fits (without allowance for resonance feed-down), for produced hadrons π , K and p and multi-strange hadrons ϕ and Ω . On the top of the plot, the numerical labels indicate the centrality selection. For π , K and p , 9 centrality bins (from top 5% to 70-80%) were used for $\sqrt{s_{NN}} = 200$ GeV Au+Au collisions [2]. The results from p+p collisions are also shown. For ϕ and Ω , only the most central results are presented. Dashed and solid lines are the 1- σ and 2- σ contours, respectively. Right plot: Ratios of p_T -integrated mid-rapidity yields for different hadron species measured in STAR for central Au+Au collisions at $\sqrt{s_{NN}} = 200$ GeV. The horizontal bars represent statistical model fits to the measured yield ratios for stable and long-lived hadrons. The fit parameters are $T_{ch} = 163 \pm 4$ MeV, $\mu_B = 24 \pm 4$ MeV, $\gamma_s = 0.99 \pm 0.07$. The variation of γ_s with centrality is shown in the inset, including the value (leftmost point) from fits to yield ratios measured by STAR for 200 GeV p+p collisions.

hadrons through multi-strange baryons, is consistent with the light flavors, u , d , and s , having reached chemical equilibrium (for central and near-central collisions only) at $T_{ch} = 163 \pm 5$ MeV. The deviations of the short-lived resonance yields, such as those for Λ^* and K^* collected near the right side of Fig. 7, from the statistical model fits, presumably result from hadronic re-scattering after the chemical freeze-out and needs to be further understood.

The saturation of the strange sector yields, attained for the first time in near-central RHIC collisions, is particularly significant. The saturation is indicated quantitatively by the value obtained for the non-equilibrium parameter γ_s for the strange sector for central collisions. The temperature deduced from the fits is essentially equal to the critical value for a QGP-to-hadron-gas transition predicted by Lattice QCD [67], but is also close to the Hagedorn limit for a hadron resonance gas, predicted without any consideration of quark and gluon degrees of freedom [68]. If thermalization is indeed achieved by the bulk matter prior to chemical freeze-out, then the deduced value of T_{ch} represents a lower limit on that thermalization temperature.

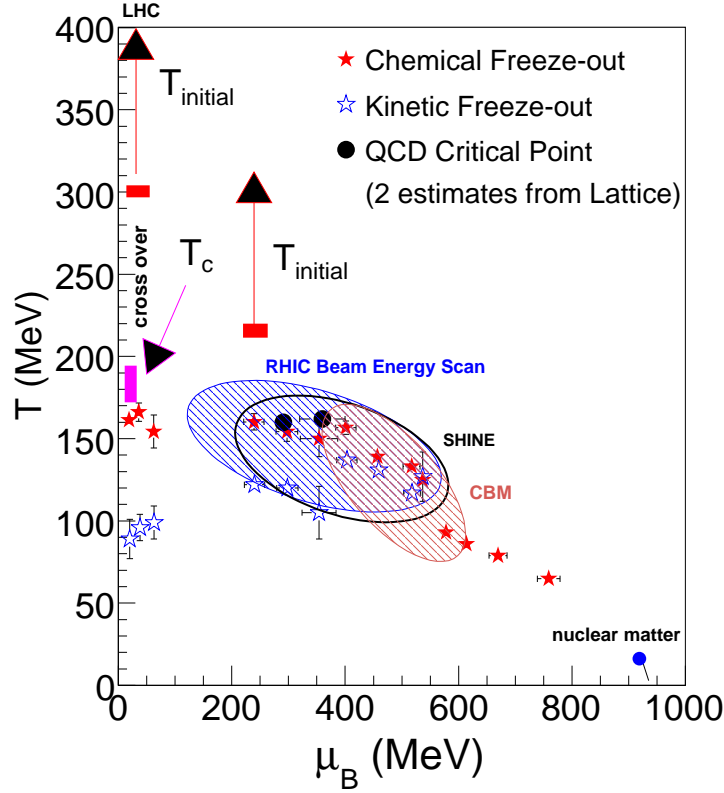


Figure 8. (Color online) Temperature vs. baryon chemical potential (μ_B) from heavy-ion collisions at various $\sqrt{s_{NN}}$ [61]. The μ_B values shown are estimated at chemical freeze-out. The kinetic and chemical freeze-out parameters, extracted using models assuming thermal and chemical equilibrium from midrapidity particle ratio and p_T spectra measurements in heavy-ion collisions. The range of critical temperatures (T_c) of the cross-over quark-hadron phase transition at $\mu_B = 0$ and the QCD critical point from two different calculations from lattice QCD are also indicated. Model-based estimates of the range of initial temperature (T_{initial}) achieved in heavy-ion collisions based in part on direct photon data at top RHIC [69] and SPS [70] energies are also shown. The range of μ_B to be scanned in the RHIC beam energy scan program corresponding to $\sqrt{s_{NN}} = 5.5$ to 39 GeV as well as experiments at SPS and CBM are indicated as shaded ellipse. The solid point around $T \sim 0$ and $\mu_B = 938$ MeV represents nuclear matter in the ground state.

5. Summary and Outlook

In summary, the current understanding of the QCD phase diagram is depicted in Fig. 8. From the QCD calculations on lattice it is now established theoretically that the quark-hadron transition at $\mu_B = 0$ is a cross-over. The critical temperature for a quark-hadron phase transition lies within a range of 170-190 MeV. Most calculations on lattice also indicate the existence of QCD critical point for $\mu_B > 160$ MeV. The exact location of CP is not yet known unambiguously. Two such predictions computed on lattice are

shown in Fig. 8 for a T_c of 176 MeV [12]. New distinct signatures have been predicted by QCD model calculations to locate the critical point in the phase diagram. The specific suggestion for a CP search is to look for non-monotonic variation in the products of the higher moments of net-proton and net-charge distributions, which are related to susceptibilities, as a function of $\sqrt{s_{NN}}$ (or T, μ_B). At top RHIC energies, fluctuations in net-proton numbers are found to be consistent with expectations from HRG and lattice QCD calculations [55]. These measurements established the baseline for the CP search in the heavy-ion collision program, put constraints on the location of CP in the QCD phase plane and added to the evidences for thermalization in central Au+Au collisions at RHIC.

High energy heavy-ion collision experiments have seen distinct signatures which suggest that the relevant degrees of freedom in the initial stages of the collisions at top RHIC energies are quark and gluons [8]. Three such signatures related to strangeness enhancement, jet quenching and partonic collectivity are discussed in this paper. The initial temperatures (T_{initial}) achieved at top RHIC and SPS energies are obtained from models [71] that explain the direct photon measurements from the PHENIX experiment at RHIC [69] and from the WA98 experiment at SPS [70]. From these models, which assume that thermalization is achieved in the collisions within a time between 0.1–1.2 fm/c, the T_{initial} extracted is greater than 300 MeV at RHIC and greater than 200 MeV at SPS. Further, the understanding of suppression in high p_T hadron production in heavy-ion collisions relative to $p+p$ collisions at RHIC requires a medium energy density $\gg 1$ GeV/fm³ (critical energy density from lattice for a phase transition). This also shows that the medium has a high degree of opacity to propagation of color charges. In addition the measurement of elliptic flow and the observation of number of constituent quark scaling demonstrates that substantial collectivity has been developed in the partonic phase. The magnitude of the flow across several hadronic species and a small value of viscosity to entropy ratio extracted from the data supports the idea of formation of a strongly coupled system in the heavy-ion collisions. This then also supports the notion of creating a liquid with low viscosity in high energy nuclear collisions [72].

The experiments have also measured the temperature at which the inelastic collisions ceases (chemical freeze-out) and elastic collisions ceases (kinetic freeze-out). These temperatures (as shown in Fig. 8) are extracted from the measured particle ratios and transverse momentum distributions using model calculations which assume the system is in chemical and thermal equilibrium.

New experimental programs at RHIC, SPS, FAIR and NICA facilities have been designed to explore a large part of the QCD phase diagram, covering a μ_B range of 20–600 MeV. Whereas the experimental program at LHC (probing the cross over region of $\mu_B \sim 0$ MeV of the phase diagram) have started to provide an unique opportunity to understand the properties of matter governed by quark-gluon degrees of freedom at unprecedented high initial temperatures (higher plasma life time) achieved in the Pb+Pb collisions at 2.76–5.5 TeV [73]. Both at LHC and RHIC, one specific observable that has the potential to provide a further understanding of system formed in heavy-ion collision

are the dileptons. Theoretically they are from the virtual photons, and are different from real photons in having a mass. The dilepton mass opens up a new dimension and can be used to study time evolution of the system in heavy-ion collisions. For example, recently it has been discussed that virtual photon (dilepton) interferometry provide access to the development of collective flow with time [74]. Studying the p_T dependence of the elliptic flow and nuclear modification factor for dileptons for masses corresponding to various hadrons and beyond will help us understand partonic collectivity and medium opacity. Comparing the spectral functions of resonances decaying to dileptons and hadrons will let us know about the medium effects. While the slope of the dilepton p_T distributions will tell us about development of radial flow and provide direct evidence of thermal radiation of partonic origin in high energy nuclear collisions [75].

5.1. Acknowledgments

I would like to thank Drs. J. Alam, S. Chatopadhyay, S. Gupta, V. Koch, L. Kumar, T. K. Nayak, P. K. Netrakanti, D. P. Mahapatra, K. Rajagopal, H. G. Ritter, M. Stephanov, Y. P. Viyogi, N. Xu and Z. Xu for useful discussions. I would like to thank C. Jena, X. F. Luo, Md. Nasim, S. Singha and Drs. M. Sharma, S. Shi and A. Tang for their help in preparation of this manuscript. This work is supported by DAE-BRNS project Scantion No. 2010/21/15-BRNS/2026.

References

- [1] T. D. Lee, Trans. N. Y. Acad. Sci. Ser.2, v.40, 0111 (1980); J. C. Collins, M. J. Perry, Phys. Rev. Lett. 34, 1353 (1975).
- [2] STAR Collaboration, B. I. Abelev et al., Phys. Rev. C 79, 034909 (2009).
- [3] The Frontiers of Nuclear Science, 2007 NSAC Long Range Plan: <http://www.sc.doe.gov/np/nsac/docs/Nuclear-Science.Low-Res.pdf>
- [4] E. V. Shuryak, Phys. Rept. 61, 71 (1980); L. D. McLerran, Rev. Mod. Phys. 58, 1021 (1986).
- [5] J. M. Lattimer and M. Prakash, Phys. Rept. 442, 109 (2007).
- [6] M. G. Alford, A. Schmitt, K. Rajagopal, T. Schafer, Rev. Mod. Phys. 80, 1455 (2008).
- [7] P. Braun-Munzinger and J. Stachel, Nature 448, 302 (2007).
- [8] BRAHMS Collaboration, I. Arsene et al., Nucl. Phys. A 757 (2005) 1; PHOBOS Collaboration, B.B. Back et al., Nucl. Phys. A 757 (2005) 28; STAR Collaboration, J. Adams et al., Nucl. Phys. A 757 (2005) 102; PHENIX Collaboration, K. Adcox et al., Nucl. Phys. A 757 (2005) 184.
- [9] Y. Aoki, G. Endrodi, Z. Fodor, S.D. Katz, K.K. Szabo, *Nature* **443** (2006) 675; F. R. Brown et al., Phys. Rev. Lett. 61, 2058 (1988).
- [10] M. Cheng et al., Phys. Rev. D 74, 054507 (2006); Y. Aoki et al., Phys. Lett. B 643, 46 (2006); S. Borsanyi et al., arXiv:1011.4330.
- [11] K. Rajagopal and F. Wilczek, arXiv:hep-ph/0011333.
- [12] M. Stephanov, Prog. Theor. Phys. Suppl. 153, 139 (2004); Int. J. Mod. Phys. A20, 4387 (2005); Z. Fodor and S.D. Katz, JHEP0404, 50 (2004); R. V. Gavai and S. Gupta, Phys. Rev. D78, 114503(2008); Phys. Rev. D71, 114014 (2005).
- [13] J. Rafelski and B. Muller, Phys. Rev. Lett. 48 (1982) 1066; P. Koch, B. Muller, J. Rafelski, Phys. Rep. 142 (1986) 167.
- [14] L. D. McLerran and T. Toimela, Phys. Rev. D 31, 545 (1985). E. V. Shuryak, Phys. Lett. B 78, 150 (1978). B. Sinha, Phys. Lett. B 197, 263 (1987).

- [15] K. Kajantie, J. I. Kapusta, L. D. McLerran, A. Mekjian, Phys. Rev. D 34, 2746 (1986); S. Raha, B. Sinha, Phys. Rev. Lett. 58, 101 (1987).
- [16] T. Matsui and H. Satz, Phys. Lett. B 178, 416 (1986).
- [17] A. Shor, Phys. Rev. Lett. 54 (1985) 1122.
- [18] S. Okubo, Phys. Lett. 5 (1963) 165; G. Zweig, CERN Report Nos. TH-401 and TH-412 (1964) (unpublished). J. Iizuka, K. Okada, and O. Shito, Prog. Theor. Phys. 35 (1966) 1061.
- [19] J. Cleymans and A. Muronga, Phys. Lett. B 388 (1996) 5; J. Cleymans, M. Marais and E. Suhonen, Phys. Rev. C 56 (1997) 2747.
- [20] J. Cleymans *et al.*, Phys. Rev. C 57 (1998) 3319; S. Hamieh, K. Redlich and A. Tounsi, Phys. Lett. B 486 (2000) 61.
- [21] K. Redlich and A. Tounsi, Eur. Phys. J. C 24 (2002) 589; A. Tounsi and K. Redlich, eprint : hep-ph/0111159.
- [22] B. I. Abelev *et al.* (STAR Collaboration), Phys. Lett. B 673 (2009) 183.
- [23] T. Akesson *et al.* (AFS Collaboration), Nucl. Phys. B 203 (1982) 27.
- [24] B. Mohanty and N. Xu, J. Phys. G 36 (2009) 064022.
- [25] B.I. Abelev *et al.* (STAR Collaboration), Phys. Rev. Lett. 99 (2007) 112301.
- [26] PHENIX Collaboration, S. S. Adler *et al.*, Phys. Rev. Lett. 91, 072301 (2003); PHOBOS Collaboration, B. B. Back *et al.*, Phys. Rev. Lett. 91, 072302 (2003); STAR Collaboration, J. Adams *et al.*, Phys. Rev. Lett. 91, 072304 (2003); BRAHMS Collaboration, I. Arsene *et al.*, Phys. Rev. Lett. 91, 072305 (2003).
- [27] X.-N. Wang, Miklos Gyulassy, Phys. Rev. Lett. 68, 1480 (1992).
- [28] I. Vitev and M. Gyulassy, Phys. Rev. Lett. 89 (2002) 252301; M. Gyulassy, P. Levai, I. Vitev, Phys. Rev. Lett. 85, 5535 (2000).
- [29] X.-N. Wang, Phys. Rev. C 70, 031901(R) (2004).
- [30] M. L. Miller, K. Reygers, S. J. Sanders, P. Steinberg, Ann. Rev. Nucl. Part. Sci. 57, 205 (2007).
- [31] STAR Collaboration, B. I. Abelev *et al.*, Phys. Rev. Lett. 97, 152301 (2006); Phys. Lett. B 655, 104 (2007); PHENIX Collaboration, A. Adare *et al.*, arXiv:1004.3532; Phys. Rev. C 82, 011902(R) (2010); Phys. Rev. Lett. 101, 232301 (2008).
- [32] S. S. Adler *et al.*, Phys. Rev. Lett. 96, 202301 (2006).
- [33] STAR Collaboration, J. Adams *et al.*, Phys. Lett. B 637, 161 (2006).
- [34] PHENIX Collaboration, A. Adare *et al.*, Phys. Rev. C 77, 064907 (2008).
- [35] PHENIX Collaboration, A. Adare *et al.*, arXiv:1005.1627v2; Phys. Rev. Lett. 98, 172301 (2007).
- [36] J. Alam *et al.*, Phys. Rev. D 71 (2005) 094016; arXiv:hep-ph/0604131.
- [37] X.N. Wang, Z. Huang and I. Sarcevic Phys. Rev. Lett. 77, 231 (1996).
- [38] M. Cacciari, J. Rojo, G. P. Salam and G. Soyez, arXiv:1010.1759
- [39] N. Armesto *et al.*, Phys. Rev. D 71, 054027 (2005); X.-N. Wang, Phys. Rev. C 58, 2321 (1998); Q. Wang and X.-N. Wang, Phys. Rev. C 71, 014903 (2005); B. Mohanty (for STAR Collaboration), arXiv:0705.0953.
- [40] J.-Y. Ollitrault, Phys. Rev. D 46, 229 (1992); H. Sorge, Phys. Rev. Lett. 82, 2048 (1999).
- [41] S.S. Shi, (for the STAR Collaboration), Nucl. Phys. A 830, 187C (2009).
- [42] C. Jena, (for the STAR Collaboration), arXiv:1101.4196 .
- [43] D. Teaney, J. Lauret, E. V. Shuryak, Phys. Rev. Lett. 86, 4783 (2001). P. Huovinen, P.F. Kolb, U. Heinz, P.V. Ruuskanen, and S.A. Voloshin, Phys. Lett. B 503, 58 (2001); C. Nonaka *et al.*, Phys. Lett. B 583, 73 (2004). T. Hirano and Y. Nara, Phys. Rev. C 69, 034908 (2004).
- [44] STAR Collaboration, J. Adams *et al.*, Phys. Rev. Lett. 92, 052302 (2004); PHENIX Collaboration, S.S. Adler *et al.*, Phys. Rev. Lett. 91, 182301 (2003).
- [45] D. Molnar and S.A. Voloshin, Phys. Rev. Lett. 91, 092301 (2003); R. J. Fries *et al.*, Phys. Rev. C 68, 044902 (2003); J.H. Chen *et al.*, Phys. Rev. C 74, 064902 (2006); V. Greco, C.M. Ko, P. Levai, Phys. Rev. Lett. 90, 202302 (2003).
- [46] Md. Nasim, *et al.*, Phys. Rev. C 82, 054908 (2010).
- [47] PHENIX Collaboration, A. Adare *et al.*, Phys. Rev. Lett. 98, 162301 (2007); STAR Collaboration,

- B.I. Abelev et al., arXiv:0909.0566; Phys. Rev. C 77, 054901 (2008).
- [48] Roy A. Lacey et al., Phys. Rev. Lett. 98, 092301 (2007); S. Gavin and M. Abdel-Aziz, Phys. Rev. Lett. 97, 162302 (2006); H-J. Drescher, A. Dumitru, C. Gombeaud, J.-Y. Ollitrault, Phys. Rev. C 76, 024905 (2007).
- [49] A. Tang, Nucl. Phys. A 830, 673C (2009).
- [50] V. Koch *et al.*, Phys. Rev. Lett. 95, 182301 (2005); M. Asakawa *et al.*, Phys. Rev. Lett. 85, 2072 (2000).
- [51] M. A. Stephanov et al., Phys. Rev. D 60, 114028 (1999).
- [52] B. Berdnikov et al., Phys. Rev. D 61, 105017 (2000).
- [53] M. A. Stephanov, Phys. Rev. Lett. 102, 032301 (2009).
- [54] M. Asakawa et al., Phys. Rev. Lett. 103, 262301 (2009).
- [55] STAR Collaboration, M. M. Aggarwal et al., Phys. Rev. Lett. 105, 022302 (2010).
- [56] R.V. Gavai and S. Gupta, Phys. Lett. B 696, 459 (2011).
- [57] F. Karsch and K. Redlich, Phys. Lett. B 695, 136 (2011).
- [58] M. Cheng et al., Phys. Rev. D 79, 074505 (2009); B. Stokic et al., Phys. Lett. B 673, 192 (2009).
- [59] Y. Hatta *et al.*, Phys. Rev. Lett. **91**, 102003 (2003).
- [60] J. Cleymans et al., Phys. Rev. C 73, 034905 (2006).
- [61] B. Mohanty, Nucl. Phys. A 830, 899c (2009).
- [62] STAR Collaboration, B. I. Abelev et al., Phys. Rev. C 81, 024911 (2010).
- [63] STAR Collaboration, J. Adams et al., Phys. Rev. Lett. 98, 062301 (2007); PHENIX Collaboration, A. Adare et al., Phys. Rev. Lett. 98, 232301 (2007).
- [64] P. Huovinen, and P.V. Ruuskanen, Ann. Rev. Nucl. Part. Sci. 56, 163 (2006).
- [65] Z. Tang et al., arXiv:1101.1912.
- [66] E. Schnedermann, J. Sollfrank, and U. Heinz, Phys. Rev. C 48, 2462 (1993).
- [67] F. Karsch, Lecture Notes in Physics 583, 209 (2002).
- [68] R. Hagedorn, Nuovo Cim. Suppl.3, 147 (1965).
- [69] PHENIX Collaboration, A. Adare et al., Phys. Rev. Lett. 104, 132301 (2010).
- [70] WA98 Collaboration, M. M. Aggarwal et al., Phys. Rev. Lett. 85, 3595 (2000).
- [71] R. Chatterjee, D. K. Srivastava and S. Jeon, Phys. Rev. C 79, 034906 (2009); P. Huovinen, P.V. Ruuskanen and S. S. Rasanen, Phys. Lett. B 535, 109 (2002); A. K. Chaudhuri, J. Phys. G 29, 235 (2003); J. Alam et al., Phys. Rev. C 63, 021901 (2001); D. d’Enterria and D. Peressounko, Eur. Phys. J. C 46, 451 (2006); J. Alam et al., J. Phys. G 34, 871 (2007).
- [72] Barbara Jacak and Peter Steinberg, Phys. Today 63N5, 39 (2010).
- [73] ALICE Collaboration, K. Aamodt et al., Phys. Lett. B 696, 30 (2011); arXiv:1011.3916; arXiv:1011.3914; ATLAS Collaboration, G. Aad et al., arXiv:1011.6182.
- [74] P. Mohanty, J. e. Alam and B. Mohanty, arXiv:1008.1112 [nucl-th].
- [75] NA60 Collaboration, R. Arnaldi et al., Phys. Rev. Lett. 100, 022302 (2008).